Temperature-dependent nanocrystal formation in Mo/Si multilayers

I. Nedelcu, R. W. E. van de Kruijs, A. E. Yakshin, and F. Bijkerk
FOM-Institute for Plasma Physics Rijnhuizen,[*] *P.O. Box. 1207, 3430 BE Nieuwegein, The Netherlands*
(Received 11 April 2007; revised manuscript received 23 October 2007; published 7 December 2007)

We investigated the nanocrystallinity of Mo/Si multilayers as a function of the Mo:Si ratio in the period using grazing incidence and wide angle x-ray diffraction, both for as-deposited samples and after thermal annealing up to 800 °C under UHV conditions. The research was performed on multilayers, as applied for extreme UV lithography with period thickness of approximately 7 nm. The as-deposited multilayer nanostructure was found to depend on the Mo to Si layer thickness ratio. For intermediate Mo fractions in the multilayer period, a four layer system is formed, with amorphous Si and polycrystalline Mo layers separated by silicide interfaces, while for low and high Mo fractions, a two component system is formed, respectively, consisting of a pure Mo layer (in the case of a high Mo fraction) or pure Si layer (low Mo fraction) separated by a single silicide interface. Using the crystallographic properties of the multilayer during annealing, we describe the continuous development of the multilayer structure and growth of the silicide interfaces. Our study has led to an explanatory model which is based on the total free energy minimization of the multilayer system. Finally, a phase transition to a crystalline silicide is observed at $T > 300$ °C. This phase transition can also be explained by minimization of the total free energy.

DOI: 10.1103/PhysRevB.76.245404 PACS number(s): 68.65.Ac, 61.10.Nz, 64.70.Kb

I. INTRODUCTION

For next generation extreme ultra violet lithography (EUVL) systems,[1] Mo/Si multilayers will be used as reflective coatings for the imaging and EUV light collecting optics. For a proper design of the optics, it is needed that the EUV optical path through a set of reflecting multilayers is well defined. Since the optical path is to a significant degree determined by the optical properties of the multilayer, including its interfacial layers, these properties should be known with high accuracy. Moreover, to achieve a high multilayer reflectivity, a good optical contrast of the materials needs to be obtained, and this requires the Mo/Si interfaces to be abrupt with normal intermixing.

It is generally known that the layer interfaces in Mo/Si multilayers are not abrupt, since intermixing and/or compound formation occurs. These naturally formed interfaces are typically several atomic layers thick and reduce the optical contrast between Mo and Si and decrease the reflectivity. Furthermore, intermixing continues at increased temperatures, an effect that can easily occur at the high EUV illumination powers that are foreseen for EUVL at so-called high volume manufacturing conditions in the ultimate industrial lithography process. In addition, a nonhomogeneous distribution of temperatures will result in nonhomogeneous changes in the layered structure, creating, e.g., optical path differences that reduce the image quality. Although it has been shown that diffusion barriers can suppress the intermixing and compound formation,[2] a full understanding of the as-deposited layered structure and its behavior at enhanced temperatures is required for proper choice of barrier layer materials and thicknesses.

In this paper, we study the Mo/Si multilayer composition as a function of the annealing temperature in order to reveal their nanostructural composition. The Mo fraction in the multilayer is varied from a low value (application, e.g., for narrow band EUV diagnostics[3]) through intermediate value (application for high reflectance EUV optics) to high value (application, e.g., for stress-compensation layers in EUV optics or broadband multilayer reflectors[4]). Besides being interesting from the application point of view, such a systematic study of the multilayer structure as a function of the Mo fraction enables more detailed understanding of the multilayer composition and structure, including its interfacial layers. For low and high Mo fractions, the layered structure and interface composition have been uniquely determined in our study by grazing incidence x-ray reflectivity (GIXR) measurements. In addition, GIXR was used to determine the evolution of the multilayer period, yielding information on the process of interface silicide formation. The change of crystallographic parameters during annealing was characterized by wide angle x-ray diffraction (WAXRD) and compared with the layered structures obtained by GIXR. Based on these measurements, a model is developed that explains the silicide formation during annealing by the availability of bulk material components and a tendency of the multilayer system to minimize its free energy. This behavior has only become obvious in this study by systematically investigating all Mo fraction ranges.

II. EXPERIMENT

Multilayers, consisting of 50 bilayers of Mo and Si, were deposited by UHV electron-beam evaporation onto 25×25 mm^2 superpolished silicon substrates. A series of multilayers with a period thickness of 6.9 nm was produced for a large range (between 0.1 and 0.8) of the Mo fraction, defined by $\Gamma = d_{Mo}/(d_{Mo}+d_{Si})$, where d_{Mo} and d_{Si} are the thicknesses of molybdenum and silicon, respectively. The base pressure during deposition was better than 2×10^{-8} mbar, the deposition system being described elsewhere.[5] Kr ions were applied during layer growth to suppress roughness development within the multilayer. As a result of this, a reflectivity of 69%

 ©2007 The American Physical Society

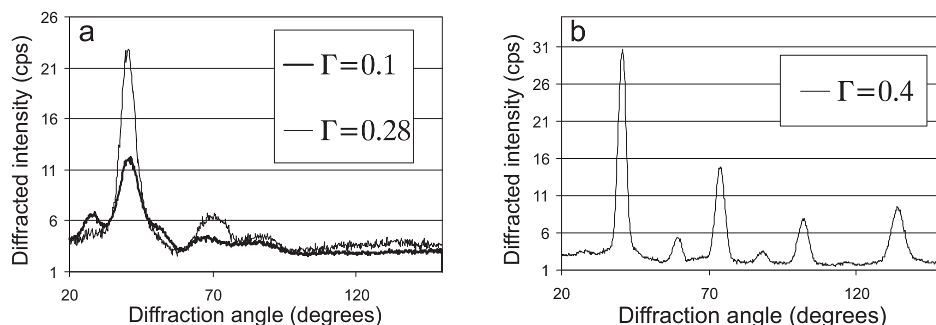

FIG. 1. (a) For $\Gamma < 0.33$, a polycrystalline Mo_3Si diffraction pattern is observed. The high background at high Γ indicates amorphous Mo or Mo_xSi_y growth. Due to the high number of diffraction peaks in the diffraction angle range of 45°–90°, the labeling of the diffraction peaks is not present in (b). All the diffraction peaks are presented in Table I. Wide angle x-ray diffraction data (b) for $\Gamma=0.4$ indicates a typical polycrystalline bcc Mo structure, which is observed for all $\Gamma > 0.33$.

is routinely achieved at 13.5 nm at near-normal incidence,[4–6] with a best value[3] of over 70%.

The multilayers were successively annealed for 48 h from 20 to 800 °C using a halogen lamp in a vacuum chamber (base pressure of 10^{-7} mbar) and analyzed by GIXR and WAXRD with a Philips X'Pert double crystal x-ray diffractometer using Cu $K\alpha$ line radiation (0.154 nm). During the WAXRD measurements, the sample was rotated by $\varphi=20°$ in the sample plane to suppress the diffraction peak from the monocrystalline substrate and aligned with the incident beam at a fixed angle of $\omega=1°$ to maximize the illuminated area and thereby the diffracted intensity. The Mo, Si, and Mo_xSi_y patterns have been identified using reference spectra from the ICCD database.[7] Reference multilayers were annealed both in successive runs at increasingly higher temperatures, as well as directly to the highest temperature to check if there is any effect of annealing history. No significant difference was observed between the two methods, and only successively annealed samples will be reported on here. Transmission electron microscopy (TEM) was used in both bright field mode (Philips CM30T) and lattice imaging mode (Philips CM300UT-FEG) at 300 kV. Specimens for TEM were prepared by Ar ion milling of multilayer cross sections glued on a copper grid.

III. EXPERIMENTAL RESULTS AND DISCUSSION

A. Nanocrystallinity of as-deposited multilayers

In this section, the spontaneous formation of Mo silicides in multilayers just upon deposition is discussed as a function of Γ with Γ in the range of 0.1–0.8. For multilayers with $\Gamma < 0.33$, the entire Mo layer is found to be converted into silicide in a reaction with Si so that the multilayer period consists of two layers. For $\Gamma > 0.33$, only a part of the Mo is consumed in that reaction to form four layers: pure Mo and Si layers and two silicide interlayers between the pure components.

Figure 1(a) shows XRD curves from multilayers with $\Gamma = 0.1$ and $\Gamma=0.28$ representative for the range $\Gamma < 0.33$. The crystallographic pattern is identified as cubic Mo_3Si.[7,8] The different diffraction peaks in the diffraction angle range of 45°–90° are presented in the figure and in Table I. The finding of Mo_3Si is in contrast with previously published results,[9,10] showing the formation of an amorphous interlayer which was suggested to be $MoSi_2$. The formation of Mo_3Si instead of $MoSi_2$, as reported here, could be connected to the deposition method used. In the case of the here applied electron-beam evaporation, the energy of the particles is in the order of 0.1 eV, while for sputter deposition, it is in the range of 1–10 eV and higher. Other parameters such as the quality of the vacuum could also influence the spontaneous formation of silicides after deposition. Experiments to determine the exact contribution of different parameters to different silicides after deposition are presently carried out.

Figure 1(b) shows an XRD spectrum from a multilayer with $\Gamma=0.4$, representative for samples in the range of 0.33–0.8, the pattern being characteristic for a Mo (bcc) polycrystalline structure. This is in agreement with previously published results for multilayers deposited by magnetron sputtering.[2,9–11]

Concerning the composition of the interlayers, Braun *et al.*[11] suggested the formation of amorphous $MoSi_2$ at both interfaces based on its low enthalpy of formation. In our earlier studies of multilayers deposited by e-beam deposition, simulations of the GIXR reflectivity indicated that the interlayer stoichiometry depends on the energy of the Kr ions[12] applied after each Si layer to smoothen the surface. For example, for multilayers with $\Gamma=0.4$ and an ion energy of 300 eV, a combination of two silicides, Mo_5Si_3 and $MoSi_2$, occurred, while for an ion energy of 2 keV, only one silicide, namely, $MoSi_2$, was found at both interfaces. These results are in agreement with a TRIM calculation[13] which shows that 2 keV Kr ions can penetrate the entire Si layer (of 4.5 nm) and reach the buried Si-on-Mo interface, while 300 eV Kr ions can penetrate only the top 1.5 nm of the Si layer being ion polished.

We have analyzed the crystallite size in the growth direction for (both Mo and Mo_3Si,) $\Gamma=0-0.28$ (Mo_3Si crystallites) and $\Gamma=0.33-1$ (Mo crystallites). This size, shown in Fig. 2, was determined from the width of the (110) diffraction peak (present in both Mo and Mo_3Si diffraction patterns), using Scherrer's formula,[14]

TABLE I. The diffraction peaks of Mo and Mo silicides from the diffraction spectra. Note that the crystallographic spectrum of Mo_3Si for $\Gamma=0.8$ at $T=800$ °C from Fig. 3 was identified as a mixture of Mo and Mo_3Si.

Structure name	*hkl*	Diffraction angle (deg)	Normalized diffracted intensity
Mo	110	40.5	1
	200	58.61	0.19
	211	73.67	0.43
	220	88.62	0.15
	310	101.42	0.24
	222	115.96	0.07
	321	132.64	0.43
h-$MoSi_2$	101	26.43	0.5
	111	41.6	1
	112	48.32	0.4
	211	63.29	0.2
	114	70.72	0.16
	301	72.8	0.16
	115	85.2	0.1
	223	98.47	0.2
	403	116.67	0.04
	411	126.98	0.12
	223	132.67	0.3
t-Mo_5Si_3	200	18.37	0.02
	220	26.08	0.05
	211	27.49	0.25
	002	36.54	0.25
	321	38.25	0.71
	202	41.18	0.38
	420	41.83	0.59
	411	42.76	1
	222	45.45	0.57
	521	54.46	0.08
	323	66.92	0.18
	631	67.84	0.12
	710	68.75	0.17
	602	69.86	0.24
	413	70.07	0.33
	642	81.92	0.11
	660	85.3	0.08
	732	86.34	0.04
c-Mo_3Si	110	25.70	0.24
	210	41.18	1
	211	45.32	0.31
	222	66.03	0.12
	320	69.11	0.17
	321	72.16	0.27
	420	89.41	0.03
t-$MoSi_2$	002	22.54	0.39
	101	29.93	0.66
	110	39.52	0.75
	103	44.45	1
	112	45.97	0.2
	200	57.13	0.2
	202	62.2	0.09
	211	65.83	0.1
	006	71.79	0.04
	213	75.13	0.29
	116	85.19	0.1

$$X = \frac{0.94\lambda}{L\cos(\theta)}, \tag{1}$$

where $\lambda=0.154$ nm, L is the full width at half maximum determined for every peak in the spectrum, and 2θ is the diffraction angle between the source and the detector. Since the diffracting planes giving rise to the (110) peak are oriented like the film plane (offset by 20°), the crystallite size in the film growth direction can be easily calculated by correcting for this offset angle. For comparison, the solid gray line in Fig. 2 indicates the deposited amount of Mo, while the dashed line indicates the thickness of the pure part of the Mo, i.e., after consumption of a part of the Mo for the formation of silicide interlayers at the Si interfaces. It is directly

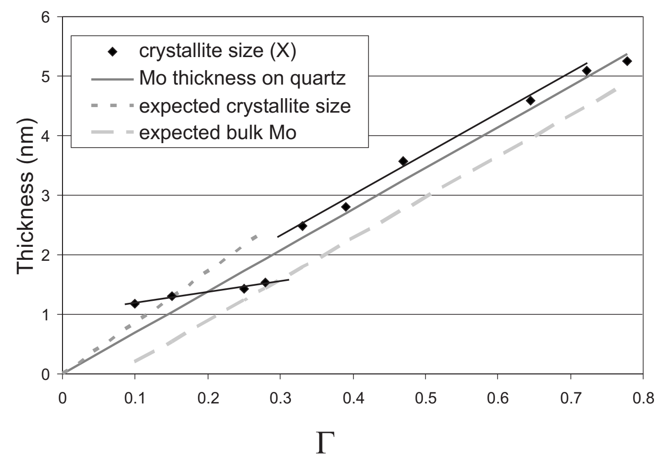

FIG. 2. Crystallite size in the growth direction as a function of the Mo fraction, compared to Mo deposited on quartz at different thicknesses. For $\Gamma<0.33$, a crystalline Mo_3Si interface is initially formed, with predominantly amorphous growth of added Mo. For $\Gamma>0.33$, the crystallite size of the period is comparable to the deposited Mo, suggesting (partly) crystalline silicide interfaces. The absence of any silicide peaks suggests amorphous interface growth.

TABLE II. Overview of silicide formation before and after annealing up to 800 °C as a function of the Mo fraction. Note that "amorphous silicides" in the range $\Gamma=0.33-0.7$ before annealing have been suggested in Ref. 12 to be a mixture of two silicides Mo_5Si_3 and $MoSi_2$. We also suggest that this part does not change at $T=300$ °C, with additional amorphous $MoSi_2$ being grown upon annealing. The crystallographic structure of amorphous silicide for $\Gamma=0.8$ at $T=400$ °C could not be uniquely identified.

<table>
<tr><th>Γ</th><th>0.1–0.28</th><th>0.33–0.35</th><th>0.4–0.5</th><th>0.6–0.65</th><th>0.7</th><th>0.8</th></tr>
<tr><td>$T=20$ °C (after deposition)</td><td>Crystalline Mo_3Si</td><td colspan="4">Amorphous silicides ($Mo_5Si_3+MoSi_2$)</td><td>Amorphous $MoSi_2$</td></tr>
<tr><td>$T=300$ °C (before h-$MoSi_2$ formation)</td><td>Crystalline Mo_3Si</td><td colspan="4">Amorphous silicides ($Mo_5Si_3+MoSi_2$) + Amorphous $MoSi_2$</td><td>Amorphous $MoSi_2$</td></tr>
<tr><td>$T=400$ °C (after h-$MoSi_2$ formation)</td><td colspan="3">Crystalline h-$MoSi_2$</td><td colspan="2">Amorphous Mo_5Si_3</td><td>Amorphous silicide</td></tr>
<tr><td>$T=800$ °C (quasiequilibrium)</td><td colspan="2">Crystalline t-$MoSi_2$</td><td colspan="2">Crystalline Mo_5Si_3</td><td colspan="2">Crystalline Mo_3Si</td></tr>
</table>

apparent that there are two regions of crystallite formation, with full crystallization occurring only for $\Gamma>0.33$.

Shown in Fig. 2 is the expected crystallite size of Mo_3Si for $\Gamma=0.1-0.28$, based on calculations assuming that all deposited Mo forms crystalline Mo_3Si (dotted line). However, our experimental data show that the increase in Mo_3Si crystallite size as a function of Γ is much smaller than these calculated values. This suggests that Mo_3Si grows crystalline only initially up to 1.5 nm, while at larger thicknesses, only amorphous growth of Mo or Mo silicide occurs. This could be caused by the formation of crystalline Mo or Mo_3Si as a function of the as deposited Mo thickness when the Mo layer is covered by the next Si layer. This will be discussed in detail in Ref. 15.

In contrast with low Γ systems, for $\Gamma>0.33$, corresponding to Mo amounts larger than 2.3 nm, the crystalline size in the growth direction seems to be comparable to the as deposited Mo layer thickness. The figure thus shows an abrupt onset of Mo crystallization above a Mo thickness of ~2.3 nm, in agreement with earlier data.[9,10] Since the formation of interfaces directly after deposition will reduce the Mo amount available for crystallization (dashed curve in Fig. 2), the observed crystallite size suggests that the Mo nanocrystals extend beyond the thickness of the pure Mo layer. It should, however, be noted that the Scherrer formula might not be fully correct to determine the size of our nanosized crystals. We have therefore also performed *ab initio* full pattern x-ray diffraction simulations for nanosized crystallites. By comparing these calculated spectra to the XRD data, we find crystal sizes that are slightly smaller than the pure Mo thickness, a result which would leave space for the assumption of amorphous interfaces. High-resolution transmission electron microscopy also suggests that both Mo-Si interfaces are amorphous, although this technique may not detect subnanometer crystallites. More detailed simulations, as well as TEM studies (energy dispersive spectroscopy and electron energy loss spectroscopy), are being carried out to properly investigate size effects of nanosized crystallites, and distinguish between the presence of crystalline and amorphous interfaces.

B. Multilayer structure at enhanced temperatures

We will discuss the multilayer behavior upon thermal treatment as a function of Γ. We have subdivided our temperature range based on major changes in the composition of multilayers considering the h-$MoSi_2$ crystallization for $T>300$ °C. Table II presents the silicide composition for multilayers with $\Gamma=0.1-0.8$ in all temperature ranges.

Figure 3 shows an overview of the multilayer crystallinity as a function of the Mo fraction ($\Gamma=0.1$, 0.35, 0.65, and 0.8) for different temperatures (20, 300, 400, and 800 °C). The corresponding spectra are presented in this single overview graph for each Mo fraction. For clarity, the data are plotted with multiplication factors of 1, 10, 100, and 1000 times. For temperatures up to 400 °C, it is convenient to distinguish three different types of multilayer structures: low Γ (0.1–0.28), intermediate Γ (0.33–0.78), and high Γ (0.8). All crystallographic structures of Mo and Mo silicides for the diffraction spectra displayed in Figs. 1 and 3 and listed in Table I were identified using reference powder diffraction spectra.[7] Note that the crystallographic spectrum of Mo_3Si for $\Gamma=0.8$ at $T=800$ °C from Table II was identified as a mixture of Mo and Mo_3Si.

1. State up to h-$MoSi_2$ *crystallization* ($T=20-300$ °C)

Annealing up 300 °C shows the following processes as a function of the Mo fraction. For multilayers with $\Gamma=0.1-0.28$, the initial nanocrystalline structure formed at room temperature does not change. For $\Gamma=0.33-0.78$, a gradual decrease of peak intensities and increase of peak widths is observed indicating a decreasing Mo crystallite size. This would suggest a gradual growth of the amorphous silicide interfaces upon annealing. This result is confirmed by TEM measurements, where the Mo-on-Si interface did

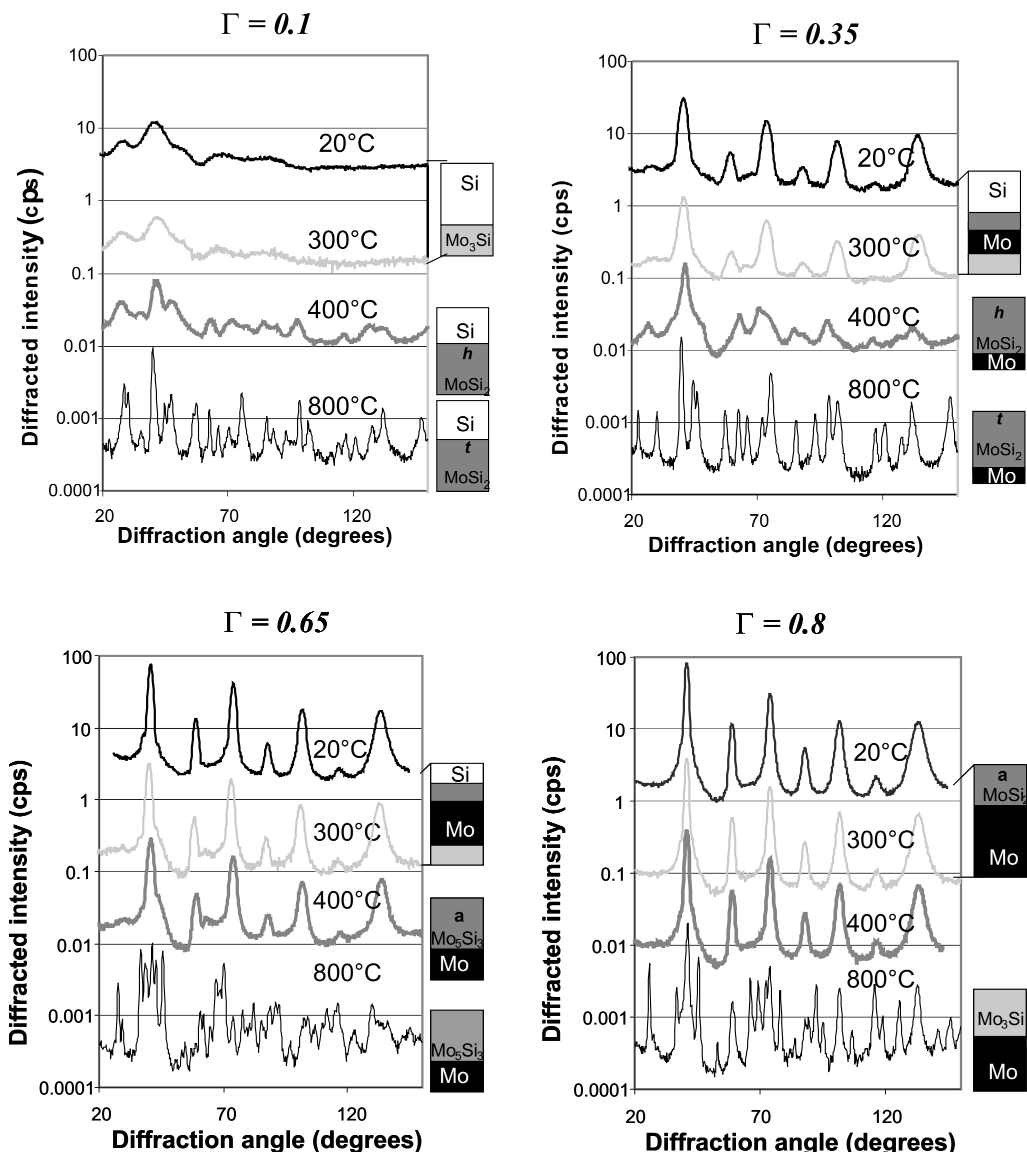

FIG. 3. Overview of wide angle x-ray diffraction data as a function of temperature. The spectra corresponding to all these temperatures are presented in the same graph for a better comparison, for each Mo fraction, by applying the same offset. For $\Gamma < 0.33$, Mo_3Si shows a phase transformation to $MoSi_2$ at 400 °C. For $\Gamma = 0.35$, a slow decrease of the Mo crystallite size (growth of the Mo_xSi_y interfaces) is followed by a phase transformation to h-$MoSi_2$. For $\Gamma = 0.6$, only a slow decrease of Mo crystallite size occurs up to 400 °C, suggesting amorphous silicide formation, but no change in the multilayer crystallographic structure. For $\Gamma = 0.8$, there is no phase transformation of the bulk Mo nor of the amorphous silicide formed after deposition. Formation of different crystalline silicides occurs at 800 °C for the investigated multilayers with $\Gamma = 0.35$, 0.6, and 0.8, respectively.

increase upon annealing, with the amount of additional silicide formed being equal to the consumed Si amount (though the thickness of the Si-on-Mo interface did not change). The only compound that would show this behavior is $MoSi_2$ based on the molecular volumes calculated from bulk atomic masses (A) and tabulated density values (R_0) for each of the compounds[16] (see Table III). It is shown in Table III that 1 nm Si and 0.4 nm Mo are consumed when forming 1 nm of $MoSi_2$, and therefore the maximum amount of $MoSi_2$ will be formed for $\Gamma_{stoichiometric} = 0.28$. For $\Gamma = 0.8$, the WAXRD patterns are identical for all temperatures up to and including 400 °C. It is difficult to obtain information about the crystallinity of interfaces because the crystalline Mo is occupying around 80 vol % of the period and dominates the WAXRD spectra. However, no change of the diffraction pattern upon annealing would suggest no crystallization of the compound formed during deposition. The GIXR measurements on as-deposited multilayers were uniquely fitted with a two layer system consisting of $Mo/MoSi_2$, which suggests that amorphous $MoSi_2$ is formed directly after deposition, e.g., as a result of Kr ions penetration through the entire 1.5 nm Si layer, in agreement with TRIM calculation.[13]

2. State after h-$MoSi_2$ crystallization ($T = 300-400$ °C)

Annealing in the range of 300–400 °C shows more pronounced processes. A clear phase transformation occurs for

TABLE III. Molecular volumes of Mo and Si existing in all Mo_xSi_y compounds are used to calculate $\Gamma_{stoichiometric}$ which is the Mo fraction corresponding to the silicide formation by total consumption of bulk components.

	A (g/mol)	R_0 (g/cm^3)	V (cm^3/mol)	V_{Mo} (cm^3/mol)	V_{Si} (cm^3/mol)	$V_{Mo}/V_{silicide}$	$V_{Si}/V_{silicide}$	$\Gamma_{stoichiometric}$ $V_{Mo}/(V_{Mo}+V_{Si})$
Mo	95.9	10.2	9.40					
Si	28.08	2.3	12.21					
Mo_3Si	315.78	8.97	35.21	28.21	12.21	0.80	0.35	0.70
Mo_5Si_3	563.74	8.2	68.75	47.01	36.63	0.68	0.53	0.56
$MoSi_2$	152.06	6.24	24.37	9.401	24.42	0.39	1.00	0.28

$\Gamma=0.1-0.5$. For $\Gamma=0.1-0.28$, the crystallographic pattern of Mo_3Si transforms into h-$MoSi_2$. For $\Gamma=0.33-0.5$, the crystallographic pattern of h-$MoSi_2$ also appears. The formation of h-$MoSi_2$, which was also previously reported,[17] could be linked to crystallization of the silicide interlayers.[9,17–19] For $\Gamma=0.6-0.78$, the small decrease of Mo crystallite size observed in the range of 20–300 °C continues up to 400 °C, suggesting continuous amorphous silicide interface formation without exhibiting the phase transformation to h-$MoSi_2$. The silicides formed cannot be identified from the diffraction pattern because they do not appear in the crystalline phase.[18] To determine the silicide formed upon annealing, we investigate the period compaction upon annealing as a function of the period thickness for three samples with $\Gamma=0.65$ in the period range of 5–10.3 nm.

Figure 4 shows the measured period compaction $d-d_0$ as a function of the initial d spacing, where d_0 and d are the multilayer period directly after deposition and after annealing at 400 °C, as determined from Bragg's law,

$$m\lambda = 2d \sin\theta\sqrt{1-\frac{2\delta}{\sin^2\theta}}, \tag{2}$$

where $m=1,2,3,\ldots$, $\delta=1-n$ is the real part of the refractive index, $\lambda=0.154$ nm is the Cu $K\alpha$ wavelength, and θ is the angle between the incident x-ray beam and the multilayer surface.

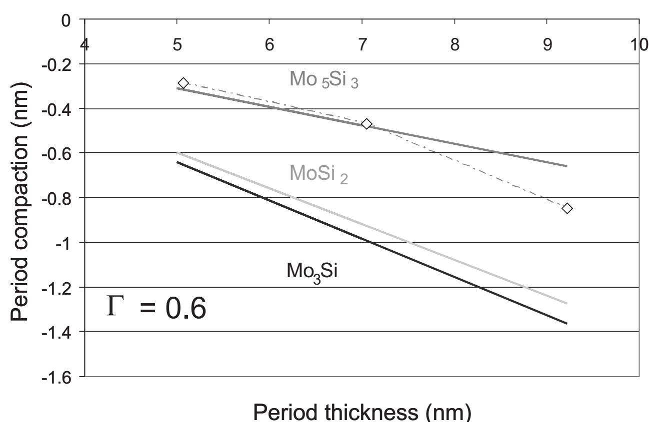

FIG. 4. Period compaction after annealing at 400 °C for multilayers with $\Gamma=0.6$ as a function of period thickness. Calculations of the expected period compaction show a best fit to the experimental data (open diamonds) for a transition to Mo_5Si_3.

Figure 4 shows experimentally measured data (open points) and the calculated period compaction, assuming a full transformation of all available Mo and Si into three different silicides: either Mo_3Si, Mo_5Si_3, or $MoSi_2$ (solid lines). Best match of the calculations to the experimental data is clearly obtained for Mo_5Si_3. Formation of silicides in the case of $\Gamma=0.8$ could not be uniquely identified because within the experimental errors, no significant changes were observed in the multilayer structure (Fig. 3).

Figure 5 displays a summary of the crystallite size in the growth direction determined from the width of the (110) diffraction peak for both Mo and h-$MoSi_2$ as a function of the annealing temperature up to 400 °C for all investigated Mo fractions. In the temperature range of 150–300 °C, only a small decrease in crystallite size for all range of Γ occurs, suggesting no change in the multilayer nanocrystallinity. For $\Gamma=0.1-0.5$ at temperatures higher than 300 °C, the crystallite size in the growth direction increases significantly [Fig. 5(a)]. This increase is proportional to the available Mo amount, with a maximum at $\Gamma_{stoichiometric}=0.28$, due to the full consumption of all available Mo and Si into $MoSi_2$, as shown in Table III. For a Mo fraction higher than 0.28, less $MoSi_2$ is formed due to a deficiency of Si in the multilayer period, and the increase in crystallite size is therefore smaller. For $\Gamma=0.6-0.8$, the crystallite size is actually decreasing [Fig. 5(b)]. This is caused by a decrease in Mo crystallite size as a result of continuing silicide formation. Note that the silicide formed does not show up at the diffraction pattern being amorphous.

3. Quasiequilibrium state ($T=800$ °C)

Annealing at 800 °C is accompanied by strong diffusion processes in which all available material has reacted. This leads to formation of new silicides in the crystalline phase.

In Fig. 3(a), different crystalline silicides are identified using references from powder diffraction files of t-$MoSi_2$ ($\Gamma=0.1$ and 0.35), Mo_5Si_3 ($\Gamma=0.65$), and Mo_3Si ($\Gamma=0.8$). If the formation of these silicides occurs according to Table III, this should lead to two types of two-layer systems: silicide/Si ($\Gamma=0.1$) and silicide/Mo ($\Gamma=0.35$, 0.65, and 0.8), depending on the available material. Indeed, after annealing the presence of Si ($\Gamma=0.1$) and Mo ($\Gamma=0.8$) besides the silicides was clearly identified.

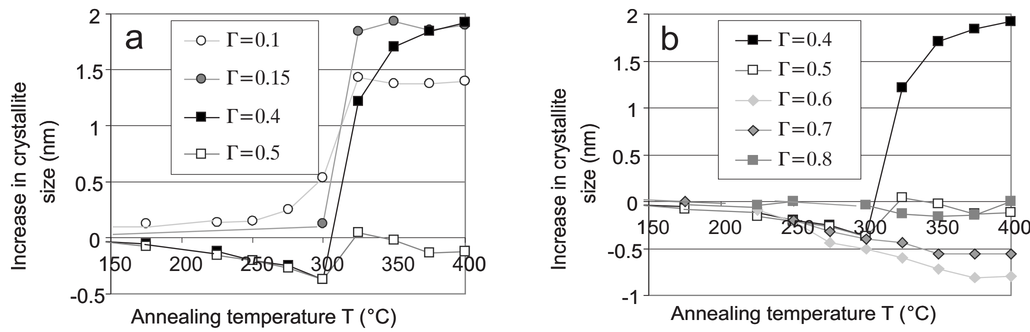

FIG. 5. Change of crystallite size in the growth direction as a function of annealing temperature for multilayers with Γ in the range of 0.1–0.8. A sudden crystallization is observed for temperatures higher than 300 °C only for multilayers with Γ in the range of 0.1–0.5. Note that the data for Γ=0.4 is shown in both figures as a reference.

Using Eq. (1), crystallite sizes of 20–30 nm are calculated, showing that crystals are penetrating through three to four periods. This is confirmed by GIXR measurements which show that the periodic nature of the multilayer is severely affected.

The silicide formation before and after annealing at 400 and 800 °C is summarized in Table II as a function of Γ. Interpretation of the process of compound formation at high temperatures is discussed in the next section.

IV. MODEL OF SILICIDE FORMATION AT ENHANCED TEMPERATURES

To understand the formation of Mo silicides upon annealing, here we present a thermodynamic model based on calculation of the most favorable energetic state of the annealed multilayer considering the available amounts of Mo and Si. The free energy due to the formation of a silicide was calculated as ΔHm, where ΔH is the enthalpy as listed in Table IV and m is the amount of formed silicide. In these calculations, the entropy can be neglected,[20] as shown in Table IV.

Figure 6 shows the total free energy as a function of the Mo fraction for the three prevailing compounds. Note that we do not distinguish between different crystallographic structures (cubic, hexagonal, and tetragonal) for Mo_5Si_3 or $MoSi_2$, because of their similar formation energies. Each curve has a minimum at the point where the available Mo and Si exactly match the amount of material required to form the compound stoichiometry. Table III displays the calculated Mo fractions ($\Gamma_{stoichiometric}$) for which all available bulk components are consumed in the formation of different silicides. From Fig. 6, we can determine the compounds with

TABLE IV. Formation enthalpies and entropies of Mo_xSi_y compounds.

Compound	ΔH (kJ/mole)	ΔS (kJ/mole)
$MoSi_2$	−44	−0.0015
Mo_5Si_3	−39	−0.0001
Mo_3Si	−28	0.0003

which the system can reach the most energetically favorable state as a function of the Mo fraction. For $\Gamma < 0.4$, this state is $MoSi_2$, for Γ in the range of 0.4–0.68, it is Mo_5Si_3, and for $\Gamma > 0.68$, it is Mo_3Si or possibly a mixture of Mo_3Si and Mo_5Si_3.

Annealing at the highest temperature applied in this work (800 °C) shows that the systems do ultimately form the predicted compounds (see Table II). Experiments also show that in the period thickness range of 5–10 nm, the final silicide stoichiometry upon annealing does depend only on Γ and not on absolute Mo or Si layer thicknesses. This proves validity of the described model. Formation of Mo_3Si instead of a mixture of Mo_3Si and Mo_5Si_3 in the case of Γ=0.8 indicates that in spite of a small difference between the free energy of the system for the cases of Mo_3Si and Mo_5Si_3, the final, most favorable state is reached. Note that we still observed the surprising spontaneous formation of crystalline Mo_3Si at room temperature in low Γ systems, an effect which is not fully understood (Sec. III A).

Results on annealing at lower temperatures (400 °C) can also be explained with the presented thermodynamic model; however, at this temperature, kinetics play a significant role. Some of the structures form silicides that correspond to stable states ($MoSi_2$ for $\Gamma < 0.4$ and Mo_5Si_3 for $\Gamma = 0.6-0.65$) or to metastable states ($MoSi_2$ for $\Gamma = 0.4-0.5$ and Mo_5Si_3 for $\Gamma = 0.7$). From our thermodynamic model, we

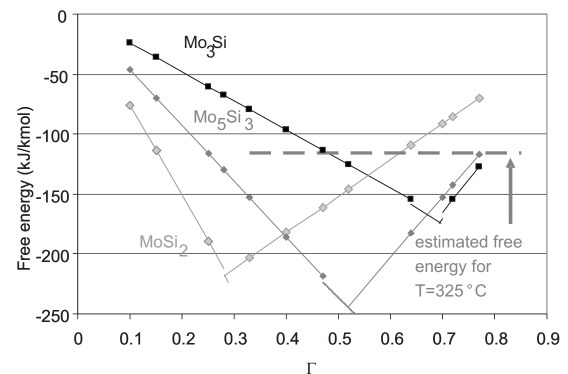

FIG. 6. Total free energy as a function of Mo fraction for the different compounds that could be formed after annealing, assuming all available material is used.

understand why certain silicides are not formed in the metastable state. To show this, we calculate the free energy of the system at $T=300\ ^\circ C$ (dashed line in Fig. 6), where all the multilayers in the range $\Gamma=0.33-0.7$ are proven to have the same structure (see Sec. III B): for this calculation, we considered 1 nm Mo_5Si_3 and 0.5 nm $MoSi_2$ interfaces that are initially formed during deposition as suggested by modeling of GIXR measurements.[12] As a result, for $\Gamma<0.45$, it is energetically favorable to convert the existing interfaces and all remaining Mo and Si into $MoSi_2$ or Mo_5Si_3, but not to Mo_3Si. At the same time, for $\Gamma>0.6$, it is energetically favorable to convert the existing interfaces and all remaining Mo and Si into Mo_3Si or Mo_5Si_3, but not to $MoSi_2$. In the range $\Gamma=0.45-0.6$, all three silicides could form.

Finally, we note that our model is based on thermodynamic properties of bulk materials; possible deviations caused by ultrathin film effects are not considered. Other effects, such as Mo crystallization for thicknesses higher than 2.3 nm or Si densification due to Kr ion treatment at $\Gamma=0.8$, should be further investigated.

V. SUMMARY

We have investigated the nanocrystallinity of Mo-Si multilayer reflecting structures of relevance for extreme UV lithography. Mo-Si multilayers of 50 periods were deposited by e-beam evaporation with a Mo fraction Γ in the range of 0.1–0.8 and annealed up to $800\ ^\circ C$. For as-deposited samples, we identified c-Mo_3Si nanocrystals at the interfaces for $\Gamma=0.1-0.25$, amorphous interfaces for $\Gamma=0.33-0.7$, and amorphous $MoSi_2$ for $\Gamma=0.8$. Upon annealing, for multilayers with $\Gamma=0.1-0.25$, a phase transformation to h-$MoSi_2$ occurs at temperatures higher than $300\ ^\circ C$. Up to $300\ ^\circ C$ multilayers with a Mo fraction in the range of 0.33–0.5 show an increase of the thickness of the naturally formed interfaces, and at higher temperatures, again the phase transformation to h-$MoSi_2$ takes place. Finally, for multilayers with $\Gamma=0.6-0.8$, amorphous Mo_5Si_3 and Mo_3Si are expected to form at low temperatures (based on experiments carried out at $400\ ^\circ C$), with a transformation to the crystalline phase observed at $800\ ^\circ C$.

In conclusion, we observe gradual growth of interfaces upon annealing to 300°, with a phase transformation occurring at higher temperatures. The final phase after annealing at high temperatures is explained by a simple model that allows the determination of the final stochiometry, based on minimization of the total free energy. This model predicts a dependence of the stochiometry on the Mo fraction, with no dependence on the multilayer period in the studied range, in agreement with all experimental results.

ACKNOWLEDGMENTS

The authors wish to thank Frans Tichelaar for the TEM measurements at Delft University of Technology. This work is part of the FOM Industrial Partnership Programme I10 ("XMO") which is carried out under contract with Carl Zeiss SMT AG, Oberkochen and the "Stichting voor Fundamenteel Onderzoek der Materie (FOM)," the latter being financially supported by the "Nederlandse Organisatie voor Wetenschappelijk Onderzoek (NWO)."

*www.rijnhuizen-nl

[1] H. Meiling, H. Meijer, V. Banine, R. Moors, R. Groeneveld, H. Voorma, U. Mickan, B. Wolschrijn, B. Mertens, G. van Baars, P. Kurz, and N. Harned, Proc. SPIE **6151**, 615108 (2006).

[2] S. Bajt, J. Alameda, T. Barbee, W. M. Clift, J. A. Folta, B. Kaufmann, and E. Spiller, Opt. Eng. (Bellingham) **41**, 1797 (2002).

[3] A. E. Yakshin, R. W. E. van de Kruijs, E. Zoethout, I. Nedelcu, E. Louis, F. Bijkerk, H. Enkisch, and S. Müllender, International EUVL Symposium, Barcelona, 2006 (http://www.sematech.org/meetings/archives/litho/euvl/7870/index.htm).

[4] E. Zoethout, G. Sipos, R. van de Kruijs, A. Yakshin, E. Louis, S. Muellender, and F. Bijkerk, Proc. SPIE **5037**, 106 (2003).

[5] E. Louis, H.-J. Voorma, N. B. Koster, F. Bijkerk, Yu. Ya. Platonov, S. Yu. Zuev, S. S. Andreev, E. A. Shamov, and N. N. Salashchenko, Microelectron. Eng. **27**, 235 (1995).

[6] E. Zoethout, P. Suter, R. W. E. van de Kruijs, A. E. Yakshin, E. Louis, F. Bijkerk, H. Enkisch, and S. Mullender, Proc. SPIE **5374**, 140 (2004).

[7] ICCD database (http://www.iccd.com).

[8] R. W. E. Kruijs, E. Zoethout, A. E. Yakshin, I. Nedelcu, E. Louis, F. Tichelaar, H. Enkisch, G. Sipos, S. Müllender, and F. Bijkerk, Thin Solid Films **515**, 430 (2005).

[9] S. Yulin, T. Feigl, T. Kuhlmann, N. Kaiser, A. I. Fedorenko, V. V. Kondratenko, O. V. Poltseva, V. A. Sevryukova, A. Yu. Zolotaryov, and E. N. Zubarev, J. Appl. Phys. **92**, 1216 (2002).

[10] S. Bajt, D. G. Stearns, and P. A. Kearney, J. Appl. Phys. **90**, 1017 (2001).

[11] S. Braun, H. Mai, M. Moss, R. Scolz, and A. Leson, Jpn. J. Appl. Phys., Part 1 **41**, 4074 (2002).

[12] A. E. Yakshin, E. Louis, P. C. Gorts, E. L. G. Maas, and F. Bijkerk, Physica B **283**, 143 (2000).

[13] J. F. Ziegler and J. P. Biersack, TRIM, Annapolis, MD, 1984–2003 (http://www.srim.org).

[14] B. E. Waren, *X-Ray Diffraction* (Dover, New York, 1999).

[15] I. Nedelcu, R. W. E. van de Kruijs, A. E. Yakshin, and F. Bijkerk (unpublished).

[16] S. P. Murarka, *Silicides For VLSI Applications* (Academic, Orlando, 1983).

[17] R. S. Rosen, D. G. Stearns, M. A. Viliardos, M. E. Kassner, S. P. Vernon, and Y. Cheng, Appl. Opt. **32**, 6975 (1993).

[18] C. Johnson, K. Anderson, A. Gromko, and D. Johnson, J. Am. Chem. Soc. **120**, 5226 (1998).

[19] V. V. Kondratenko, Yu. P. Perschin, O. V. Poltseva, A. I. Fedorenko, E. N. Zubarev, S. A. Yulin, I. V. Kozhevnikov, S. I. Sagitov, V. A. Chirkov, V. E. Levashov, and A. V. Vinogradov, Appl. Opt. **32**, 1811 (1993).

[20] F. R. de Boer, R. Boom, W. C. M. Mattens, A. R. Miedema, and A. K. Niessen, *Cohesion in Metals: Transition metal alloys* (North-Holland, Amsterdam, 1988).